Inorg. Chem. **2005**, *44*, 4915–4922

Mössbauer, Electron Paramagnetic Resonance, and Crystallographic Characterization of a High-Spin Fe(I) Diketiminate Complex with Orbital Degeneracy

Sebastian A. Stoian,[†] Ying Yu,[‡] Jeremy M. Smith,[‡] Patrick L. Holland,*[,‡] Emile L. Bominaar,*[,†] and Eckard Münck*[,†]

Department of Chemistry, Carnegie Mellon University, Pittsburgh, Pennsylvania 15213, and Department of Chemistry, University of Rochester, Rochester, New York 14627

Received March 2, 2005

The synthesis and X-ray structure of the low-coordinate, high-spin Fe^{I} compound LFe(HCCPh) (L = HC(C[^{t}Bu]N-[2,6-diisopropylphenyl])$_2$]$^-$), **1**, are reported. Low-temperature Mössbauer and electron paramagnetic resonance (EPR) spectroscopies reveal that the electronic ground state is a Kramers doublet with uniaxial magnetic properties (effective g values $g_x = 8.9$, $0 < g_y, g_z < 0.3$) that is well isolated from the excited states. The observation of a large and positive magnetic hyperfine field, $B_{int} = +68.8(3)$ T, demonstrates that the orbital angular moment is essentially unquenched along one spatial direction. Relaxation rates obtained from variable-temperature Mössbauer spectra were fit to an Orbach process, yielding $\Delta = 130–190$ cm^{-1} for the energy gap ("zero-field splitting") between the two Kramers doublets of the $S = {}^3/_2$ multiplet. Density functional theory (DFT) and time-dependent DFT calculations give insight into the electronic structures of the ground and excited states. The oxidation state of the iron and the bond order of the phenylacetylene ligand in complex **1** are analyzed using DFT, showing a substantial back-bonding interaction. Spin–orbit coupling acting in the subspace of quasi-degenerate z^2 and yz orbitals provides a consistent description of both the zero-field splitting and magnetic hyperfine parameters that fits the EPR and Mössbauer data for **1**. Interestingly, the spin–orbit coupling involves the same two orbitals (z^2, yz) as in the analogous three-coordinate Fe^{II} compounds, because back-bonding significantly lowers the energy of the xy orbital, making it the lowest doubly occupied d orbital. Despite the different oxidation state and different number of atoms in the first coordination sphere, the electronic structure of LFe^{I}(HCCPh) can be interpreted similarly to that of three-coordinate Fe^{II} diketiminate complexes, but with a substantial effect of back-bonding. To our knowledge, this is the first detailed Mössbauer and EPR study of a structurally characterized high-spin Fe^{I} complex.

Introduction

Coordination complexes of iron are ubiquitous in organometallic and biological chemistry, but iron is rarely found in the +1 oxidation state. In particular, high-spin Fe^{I} complexes are quite rare,[1] and until recently, literature examples contained dithiolene or nitrosyl ligands that yield complexes in which the oxidation state of iron is somewhat ambiguous.[2,3] In the past few years, synthetic efforts in various laboratories have led to crystallographically characterized Fe^{I} complexes with low coordination numbers.[4,5] In one case, the high-spin configuration has been confirmed using solid-state magnetic susceptibility.[4b] However, none

* Authors to whom correspondence should be addressed. E-mail: emunck@cmu.edu (E.M.); eb7g@andrew.cmu.edu (E.L.B.); holland@chem.rochester.edu (P.L.H.).

[†] Carnegie Mellon University.

[‡] University of Rochester.

(1) Hawker, P. N.; Twigg, M. V. In *Comprehensive Coordination Chemistry*; Wilkinson, G., Grillard, R. D., McCleverty, J. A., Eds.; Pergamon: New York, 1987, Vol. 4, p 1179.

(2) Williams, R.; Billig, E.; Waters, J. H.; Gray, H. B. *J. Am. Chem. Soc.* **1966**, *88*, 43−50.

(3) (a) Dance, I. G.; Miller, T. R. *Inorg. Chem.* **1974**, *13*, 525−535. (b) Connelly, N. G.; Gardner, C. *J. Chem. Soc., Dalton Trans.* **1976**, 1525−1527. (c) Stokes, S. L.; Davis, W. M.; Odom, A. L.; Cummins, C. C. *Organometallics* **1996**, *15*, 4521−4530. (d) Formally iron(I)−nitrosyl complexes are best viewed as Fe^{3+}−NO^-: Wanat, A.; Schneppensieper, T.; Stöchel, G.; van Eldik, R.; Bill, E.; Wieghardt, K. *Inorg. Chem.* **2002**, *41*, 4−10.

(4) (a) Brown, S. D.; Betley, T. A.; Peters, J. C. *J. Am. Chem. Soc.* **2003**, *125*, 322−323. (b) Betley, T. A.; Peters, J. C. *J. Am. Chem. Soc.* **2004**, *126*, 6252−6254.

(5) Kisko, J. L.; Hascall, T.; Parkin, G. *J. Am. Chem. Soc.* **1998**, *120*, 10561−10562.

10.1021/ic050321h CCC: $30.25
Published on Web 06/04/2005

of the synthetic complexes reported to have a high-spin $3d^7$ configuration have been subjected to spectroscopic inquiry using electron paramagnetic resonance (EPR) and Mössbauer spectroscopy to gain insight into the electronic structure. EPR and Mössbauer characterizations have been reported for minority Fe^{I} species observed in γ-irradiated Fe^{II} ion impurities in octahedral crystal sites[6] and ^{57}Co decay products.[7]

We are presently studying the electronic structure of LFeNNFeL (L = HC(C[^{t}Bu]N[2,6-diisopropylphenyl])$_2$]$^-$), a formally diiron(I) complex containing an activated N_2 ligand.[8] Ongoing Mössbauer studies of this dimer have revealed local sites with substantial unquenched orbital angular momentum, similar to that reported by us for Fe^{II} diketiminate complexes.[9] For the latter, orbital degeneracies give rise to isolated (quasi) doublets with uniaxial ($\mu_z \gg \mu_x$, μ_y) magnetic properties. Such properties entail exchange interactions of the Ising type, $JS_{1z}S_{2z}$,[10] quite different from that commonly described by isotropic exchange, $JS_1 \cdot S_2$. The unusual Mössbauer spectra of LFeNNFeL prompted us to study monomeric Fe^{I} diketiminate complexes to evaluate the electronic structure of the local Fe^{I} sites. We report here the *mononuclear* low-coordinate Fe^{I} compound LFe(HCCPh) (**1**) and demonstrate by use of Mössbauer spectroscopy and EPR that it has a high-spin ($S = {}^3/_2$) $3d^7$ configuration with near orbital degeneracy. We find that its magnetic properties are dominated by unquenched orbital angular momentum, like those reported by us for Fe^{II} diketiminate complexes.[9] Our work on **1** and other Fe^{I} diketiminate complexes has revealed unusual behavior of the isomer shifts; we will report these findings together with quadrupole splitting analyses in a future publication. In the present paper, we focus on the magnetic properties of complex **1**.

Materials and Methods

Compounds were synthesized and purified using standard air-free techniques, and X-ray structures used a standard area detector system, as described in detail elsewhere.[11] Mössbauer samples were transported in specially designed Delrin cells with tight-fitting caps (shrink fits), which were kept at 77 K during transport from Rochester to Pittsburgh inside capped test tubes. Toluene solutions for EPR spectroscopy were kept in flame-sealed quartz tubes. The preparation and properties of LFeCl and LFeNNFeL were previously reported.[8,12]

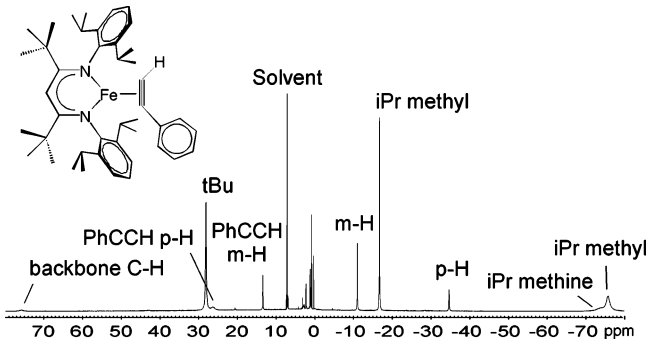

Figure 1. ^{1}H NMR spectrum of LFe(HCCPh) in benzene-d_6 at 298 K.

LFe(HCCPh). A Schlenk flask was loaded with LFeNNFeL (100 mg, 87 μmol) and pentane (6 mL). Phenylacetylene (19 μL, 175 μmol) was added via a syringe to the dark purple-red solution, resulting in immediate effervescence and the formation of a dark orange-red solution. The solution was stirred at room temperature for 30 min and concentrated to 2 mL. Vapor diffusion of the pentane into hexamethyldisiloxane at −35 °C gave dark red needles (80 mg, 70%). ^{1}H NMR (400 MHz, C_6D_6): 77 (1H, backbone C−H), 29 (18H, ^{t}Bu), 26 (1H, PhCCH p−H), 14 (2H, PhCCH m−H), −11 (4H, m−H), −17 (12H, ^{i}Pr methyl), −35 (2H, p−H), −75 (4H, ^{i}Pr methine), −77 (12H, ^{i}Pr methyl) ppm. IR (KBr pellet): 1720 cm^{-1} (C≡C). UV−vis (pentane): 338 (ϵ = 15.8 mM^{-1}cm^{-1}), 409 (ϵ = 6.0 mM^{-1}cm^{-1}), 554 (ϵ = 0.6 mM^{-1}cm^{-1}), 755 (ϵ = 0.3 mM^{-1}cm^{-1}) nm. Elem Anal. Calcd for $C_{43}H_{59}N_2Fe$: C, 78.22; H, 9.01; N, 4.25. Found: C, 78.05; H, 9.33; N, 4.33.

Mössbauer spectra were recorded on two spectrometers, using Janis Research Super-Varitemp Dewars that allowed studies in applied magnetic fields up to 8.0 T in the temperature range from 1.5 to 200 K. Mössbauer spectral simulations were performed using the WMOSS software package (WEB Research, Edina, MN). Isomer shifts are quoted relative to Fe metal at 298 K. EPR spectra were recorded on a Bruker EPR 300 spectrometer equipped with an Oxford ESR 910 liquid helium cryostat and an Oxford temperature controller.

The density functional theory (DFT) calculations were performed with the Gaussian'03 (revision B.05) software package (see Ref. S.1 in the Supporting Information), using Becke's three-parameter hybrid functional B3LYP and basis set 6-311G. The SCF calculations and geometry optimizations used tight and default convergence criteria, respectively. The stability of the ground states was tested by performing temperature-dependent DFT (TD-DFT) calculations; all excitation energies were positive when the DFT solution was used as the reference state. A Mulliken population analysis was employed to monitor electronic charge and spin distributions.

Results

Synthesis, Structure, and Proton NMR Spectroscopy. The addition of phenylacetylene to a pentane solution of LFeNNFeL gave thermally stable LFe(HCCPh), and this neutral iron(I) compound was isolated in 70% yield. Odd-electron systems often have broad, unresolved ^{1}H NMR spectra, but LFe(HCCPh) exhibits distinct peaks from −77 to +77 ppm (Figure 1). This large chemical shift dispersion was previously seen in three-coordinate Fe^{II} complexes that possess highly anisotropic magnetic properties and in three-

(6) (a) Bleaney, B.; Hayes, W. *Proc. Phys. Soc. (London)* **1957**, *B70*, 626−628. (b) Hall, T. T. P.; Hayes, W.; Stevenson, R. W. H.; Wilkens, J. *J. Chem. Phys.* **1963**, *39*, 35−39.
(7) Tuckzek, F.; Spiering, H.; Gütlich, P. *Phys. Rev. B* **1990**, *41*, 10933−46.
(8) Smith, J. M.; Lachicotte, R. J.; Pittard, K. A.; Cundari, T. R.; Lukat-Rodgers, G.; Rodgers, K. R.; Holland, P. L. *J. Am. Chem. Soc.* **2001**, *123*, 9222−9223.
(9) (a) Andres, H.; Bominaar, E. L.; Smith, J. M.; Eckert, N. A.; Holland, P. L.; Münck, E. *J. Am. Chem. Soc.* **2002**, *124*, 3012−3025. (b) Reiff, W. M.; LaPointe, A. M.; Witten, E. H. *J. Am. Chem. Soc.* **2004**, *126*, 10206−10207.
(10) (a) Mironov, V. S.; Chibotaru, L. F.; Ceulemans, A. *J. Am. Chem. Soc.* **2003**, *125*, 9750−9760. (b) Mironov, V. S.; Chibotaru, L. F.; Ceulemans, A. *Phys. Rev. B* **2003**, *67*, 14424.
(11) Holland, P. L.; Cundari, T. R.; Perez, L. L.; Eckert, N. A.; Lachicotte, R. J. *J. Am. Chem. Soc.* **2002**, *124*, 14416−14424.
(12) (a) Smith, J. M.; Lachicotte, R. L.; Holland, P. L. *Chem. Commun.* **2001**, 1542−1543. (b) Smith, J. M.; Lachicotte, R. J.; Holland, P. L. *Organometallics* **2002**, *21*, 4808−4814.

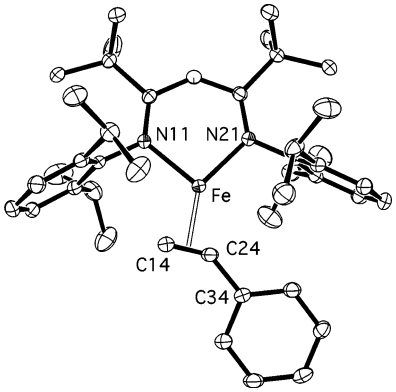

Figure 2. ORTEP drawing of the molecular structure of LFe(HCCPh). Thermal ellipsoids are shown at 50% probability. Important bond distances (Å) and angles (deg): Fe−N11 2.0049(12), Fe−N21 1.9756(12), Fe−C14 1.9291(16), Fe−C24 1.9662(15), C14−C24 1.274(2); C14−C24−C34 141.69(15), N11−Fe−N21 96.16(5).

coordinate Co^{II} complexes.[13] All proton resonances, except the acetylenic proton, can be assigned by their relative intensities (peak assignments are listed in the Materials and Methods section). The seven proton signals from the β-diketiminate ligand of this Fe^{I} compound are paramagnetically shifted in the same directions as those in the Fe^{II} compound LFeCl [LFe(PhCCH)/LFeCl resonances at 77/102 for backbone C−H, 29/43 for CH_3, −11/0 for *meta*-H, −17/−29 for ^{i}Pr CH_3, −35/−111 for *para*-H, −75/−116 for ^{i}Pr C−H, and −77/−115 for ^{i}Pr CH_3]. This similarity is explained below as a result of a similarly oriented internal magnetic field in both the Fe^{I} and Fe^{II} complexes.

The X-ray crystal structure of **1** is shown in Figure 2. The C≡C bond is elongated to 1.274(2) Å from 1.20 Å in free PhCCH,[14] and the C≡C−C angle is bent substantially to 142°. These metric data suggest back-bonding from iron to acetylene, analogous to that observed in diketiminate-supported Fe−N_2 complexes.[8] Back-bonding is also evident from the low C≡C stretching frequency of 1720 cm^{-1}, compared to 2110 cm^{-1} in PhCCH.[15] Below, these data will be discussed in more detail in the context of DFT calculations. The C≡C bond of the acetylene ligand is nearly coplanar with the N−Fe−N plane rather than in the perpendicular orientation. Steric effects favor the placement of substituents in the diketiminate plane, as we have observed for iron and nickel complexes of L and closely related complexes.[16] Therefore, it is possible that the particular orientation derives from the steric profile of the bulky diketiminate.

Mössbauer Spectroscopy. In the following, we present Mössbauer and EPR evidence that **1** is a high-spin ($S = {}^{3}/_{2}$) 3d^{7} system with orbital degeneracy. In the Discussion section, we will demonstrate that such a system produces an isolated ground doublet with the observed magnetic properties.

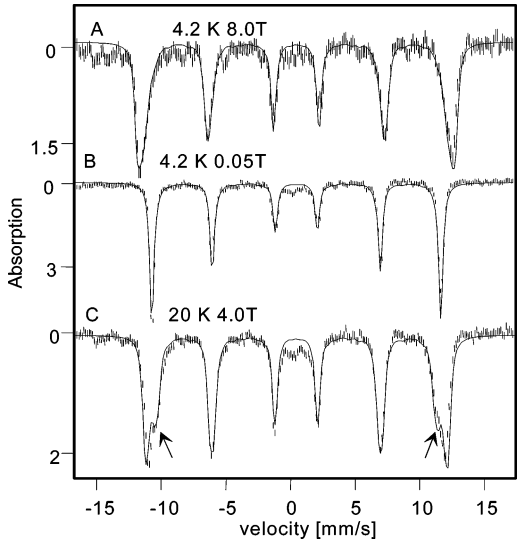

Figure 3. Low-temperature spectra of solid **1**. (A) 4.2 K, 8.0 T parallel applied field; (B) 4.2 K, 0.05 T; (C) 20 K, 4.0 T. Solid lines are spectral simulations based on eq 1. Arrows in C mark the spin-up contribution in outer lines. Isomer shift $\delta = 0.50$ mm/s relative to Fe metal at 298 K.

Figure 3 shows low-temperature Mössbauer spectra of solid **1**. The six-line pattern of Figure 3B is indicative of an electronic ground state consisting of a uniaxial Kramers doublet with effective g values $g_x \gg g_y, g_z$.[17] Spectra recorded at 4.2 K in parallel and transverse applied fields of 0.05 T (not shown) are identical. This observation, as well as spectral simulations, indicates that g_x is at least 30 times larger than g_y and g_z. A 0.05 T spectrum recorded at 22 K, shown in Figure 4, was essentially identical to that of Figure 3B, showing that, at 22 K, no other doublet is measurably populated. The magnetic splitting in spectrum 3B corresponds to an internal field of $B_{int} = 68.8(3)$ T, which is among the largest of hyperfine fields observed for iron compounds.[9,18] In the presence of an applied field, B, the magnetic splitting increases (Figure 3A), demonstrating that B_{int} is positive; this observation reveals that B_{int} is dominated by orbital contributions.[9]

The magnitude and sign of B_{int}, taken together, suggest unquenching of orbital angular momentum by spin−orbit coupling acting between a pair of nearly degenerate orbital states. We have shown for Fe^{II} diketiminate complexes that such a situation may generate a doublet with uniaxial magnetic properties.[9] The 4.0 T spectrum of Figure 3C, recorded at 20 K, exhibits two subcomponents, namely, a component with $B_{int} > 0$ belonging to the spin-down state ($M' = -{}^{1}/_{2}$) and one with $B_{int} < 0$ (arrows) belonging to the spin-up state ($M' = +{}^{1}/_{2}$), where we have described the ground doublet by fictitious spin $S' = {}^{1}/_{2}$ quantized along x to conform to the crystal field analysis presented below. Because of the large Zeeman splitting at $B = 4.0$ T, the spin-

(13) Holland, P. L.; Cundari, T. R.; Perez, L. L.; Eckert, N. A.; Lachicotte, R. J. *J. Am. Chem. Soc.* **2002**, *124*, 14416−14424.
(14) *CRC Handbook of Chemistry and Physics*, 74th ed.; Lide, R. D., Ed.; CRC Press: Boca Raton, FL, 1993; Average crystallographic value for specific type of bond, p 9-1.
(15) Kolodziejki, M.; Waliszewska, G.; Abramczyk, H. *J. Phys. Chem. A* **1998**, *102*, 1918−1926.
(16) (a) Eckert, N. A.; Bones, E. M.; Lachicotte, R. J.; Holland, P. L. *Inorg. Chem.* **2003**, *42*, 1720−1725. (b) Eckert, N. A.; Smith, J. M.; Lachicotte, R. J.; Holland, P. L. *Inorg. Chem.* **2004**, *43*, 3306−3321. (c) Vela, J.; Vaddadi, S.; Cundari, T. R.; Smith, J. M.; Gregory, E. A.; Lachicotte, R. J.; Flaschenriem, C. J.; Holland, P. L. *Organometallics* **2004**, *23*, 5226−5239.
(17) Münck, E. In *Physical Methods in Bioinorganic Chemistry*; Que, L., Jr., Ed.; University Science Books: Sausalito, CA, 2000.
(18) Reiff, W. M.; Frommen, C. M.; Yee, G. T.; Sellers, S. P. *Inorg. Chem.* **2000**, *39*, 2076−2079.

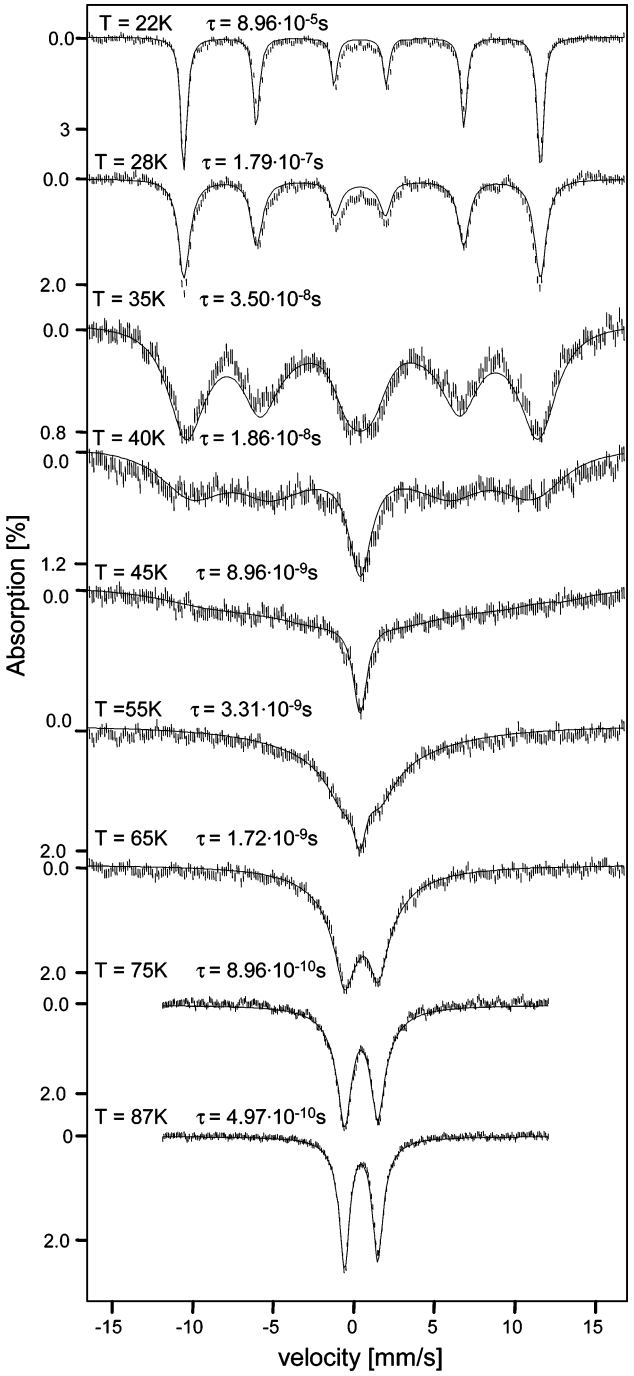

Figure 4. Variable-temperature Mössbauer spectra of solid **1** recorded in a parallel field of 0.05 T. $1/\tau$ is the stochastic flip rate of the electronic spin.

up state is only marginally populated at 4.2 K. An analysis of the relative intensities of the two subspectra of Figure 3C yields $g_x\beta B \sim 14$ cm^{-1} for $B = 4.0$ T, implying that $g_x \sim 7$. The observation of distinct spectra for the spin-up and spin-down states, as well as the observation of EPR signals for solid **1** at temperatures as low as 2.2 K (see below), shows that solid **1** is a paramagnet rather than a magnetically ordered complex.

Between 20 and 90 K, the Mössbauer spectra exhibit paramagnetic relaxation with features typical for an isolated Kramers doublet. At 150 K, the electronic spin relaxation is fast on the time scale of Mössbauer spectroscopy and the zero-field spectrum of **1** consists of one doublet (Figure S.1, Supporting Information) with $\Delta E_Q = 2.05(2)$ mm/s and $\delta = 0.44(1)$ mm/s [$\Delta E_Q = 2.02(2)$ mm/s at 180 K]. The magnetic pattern in Figure 3B is nearly symmetric, showing that the component of the electric field gradient (EFG) tensor along B_{int} is (nearly) zero. Hence, the two major components of the EFG are perpendicular to the easy magnetization axis (x) and the asymmetry parameter of the EFG must be $\eta \approx 1$. An analysis of an 8.0 T spectrum recorded at 150 K (Figure S.1) yields, accordingly, $\eta \approx 0.9$.

The low-temperature spectra of **1** were analyzed with the $S' = {}^1/_2$ spin Hamiltonian

$$\mathscr{H} = \beta\mathbf{B}\cdot\mathbf{g}\cdot\hat{\mathbf{S}}' + \frac{eQV_{zz}}{12}\left[3\hat{I}_z^{\,2} - \frac{15}{4} + \eta(\hat{I}_x^{\,2} - \hat{I}_y^{\,2})\right] - g_n\beta_n\mathbf{B}\cdot\hat{\mathbf{I}} + \hat{\mathbf{S}}'\cdot\mathbf{A}\cdot\hat{\mathbf{I}} \quad (1)$$

The quantities in eq 1 have their conventional meanings,[19] and $\Delta E_Q = (eQV_{zz}/2)(1 + \eta^2/3)^{1/2}$. Although the anisotropy of **g** directs B_{int} at 4.2 K along x, the spectrum of Figure 3B is independent of the value of g_x (because $g_x \gg g_y, g_z$).

Figure 4 shows low-field Mössbauer spectra recorded in a wide range of temperatures. It can be seen that the spectra undergo relaxation broadening above 25 K. Increased relaxation of the electronic system by spin flips between the fictitious $M' = +{}^1/_2$ and $-{}^1/_2$ spin levels then leads to a collapse of the magnetic hyperfine pattern, resulting in quadrupole doublets above 70 K. The spectral pattern observed is well-documented in the Mössbauer literature; in particular, Wickman et al.[20] have described the relaxation theory for the present situation. In the Wickman model, the fluctuation of B_{int} can be described by a single relaxation parameter τ. For $\tau > 10^{-6}$ s and $\tau < 10^{-9}$ s, the Mössbauer spectra are recorded in the slow and fast fluctuation limit, respectively, where they are insensitive to τ; in the present case, the temperature window with intermediate relaxation is 20 K $< T <$ 90 K.

The solid lines drawn through the spectra of Figure 4 represent spectral simulations with τ as the only adjustable parameter. Figure 5 shows a plot of the spin flip rate $1/\tau$ versus temperature. We have analyzed the data of Figure 5 using eq 2 (eq 1.139 of ref 21), where the first term describes the direct process, the second one describes Raman relaxation, and the last one describes Orbach relaxation.

$$\frac{1}{\tau} = a\coth\left(\frac{h\nu}{2kT}\right) + bT^9 + \frac{c}{\exp\left(\frac{\Delta}{kT}\right) - 1} \quad (2)$$

In eq 2, a, b, and c are adjustable constants, $h\nu$ is the Zeeman splitting of the ground doublet, and Δ is the energy of the

(19) Gütlich, P.; Link, R.; Trautwein, A. X. *Mössbauer Spectroscopy and Transition Metal Chemistry − Inorganic Chemistry Concepts 3*; Springer-Verlag: Berlin, 1978.
(20) (a) Wickman, H. H.; Wertheim, G. K. In *Chemical Applications of Mössbauer Spectroscopy*; Goldanskii, V. I., Herber, R. H., Eds.; Academic Press: New York, 1968. (b) Wickman, H. H.; Klein, M. P.; Shirley, D. A. *Phys. Rev.* **1966**, *152*, 345−357. (c) Wickman, H. H.; Wafner, C. F. *J. Chem. Rev.* **1969**, *51*, 435.
(21) Abragam, A.; Bleaney, B. *Electron Paramagnetic Resonance of Transition Ions*; Dover: New York, 1986.

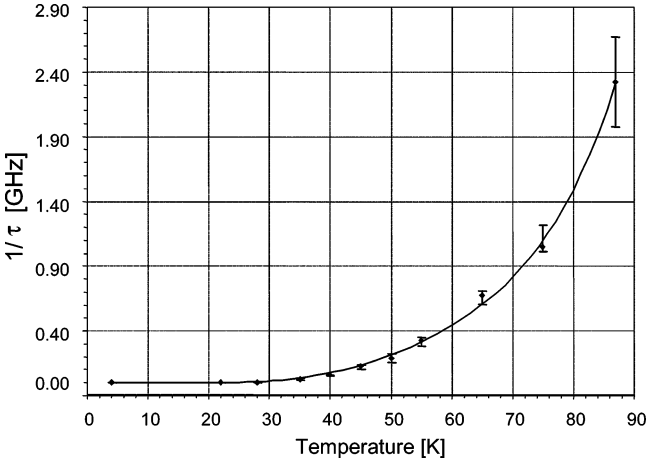

Figure 5. Variation of $1/\tau$ with temperature obtained by the spectral simulations shown in Figure 4. The error bars indicate the range of values of the relaxation rate for which reasonable simulations are obtained. The solid line is a fit obtained using eq 2 with $a = 0.0$, $b = 4.57 \times 10^{-16}$ $s^{-1}K^{-9}$, $c = 1.17 \times 10^{5}$ s^{-1}, and $\Delta = 136$ cm^{-1}, see text.

excited doublet that can be transiently populated by phonon absorption from one member of the ground doublet followed by phonon emission to the other member, effectively flipping the fictitious spin S' of the ground doublet and the associated internal field, $B_{int} = -\langle S'_x \rangle A_x / g_n \beta_n$, at the Mössbauer nucleus. The Orbach process often dominates at temperatures where the relaxation is intermediate, providing a means to determine Δ. When a computer program described by Schultz and co-workers was used,[22] the Mössbauer spectra of Figure 4 were simulated by adjusting the relaxation parameter τ to give the best agreement with the data. The analysis of the resulting $1/\tau(T)$ curve, shown in Figure 5, indicates that the direct process has a negligible influence on the spectra and that the Orbach process is the dominant relaxation mechanism in the temperature range 20 K $< T <$ 70 K. At higher temperatures, the Raman process provides the most effective relaxation pathway. Unfortunately, only the 75 and 87 K spectra of Figure 4 are sensitive to the Raman process and, thus, the parameters b and c are strongly correlated. The data collected between 20 and 65 K can be fitted for $a = b = 0$ to an Orbach process, yielding $\Delta = 180$ cm^{-1}. Extending the temperature range to 87 K and allowing Raman relaxation yields $\Delta = 136$ cm^{-1}; this fit is shown in Figure 5. (For $\Delta = 150$ cm^{-1}, the excited doublet would have 10% population at 87 K; neglecting this population should have a negligible effect on the spectra, in particular, because the Mössbauer spectra of the excited doublet are expected to be similar to those of the ground state; see Discussion.)

In Figure S.1 (Supporting Information), we present an 8.0 T spectrum with fast relaxation, recorded at 150 K. At this temperature, the excited state at energy Δ is appreciably populated. The shape of the spectrum indicates that the magnetic hyperfine field is uniaxial, that is, $|B_{int}(x)| \gg |B_{int}(y)|$, $|B_{int}(z)|$, and that this property is not affected by populating the excited state. A simulation of the 8 T, 150 K spectrum yields $\eta \approx 0.9$ for the asymmetry parameter of the EFG, in agreement with the value obtained from the analysis of the 4.2 K spectra (cf. Supporting Information).

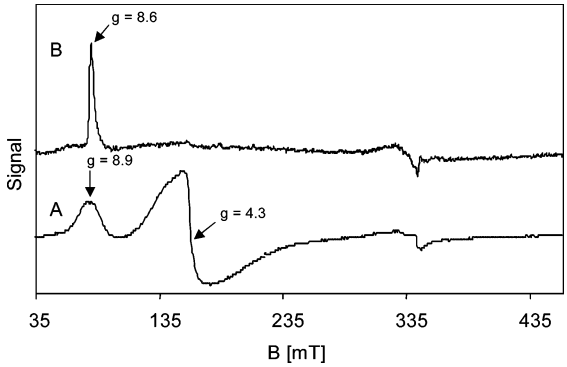

Figure 6. X-band EPR spectra of solid **1** (A) and **1** dissolved in toluene (B). Conditions: 9.63 GHz, 0.94 mT modulation amplitude, 2 mW (A) or 0.2 mW (B) microwave power, $T = 4.6$ K for A and $T = 7$ K for B. The $g = 4.3$ signal is due to a contaminant.

EPR Studies. We have studied X-band EPR spectra of **1** between 2.2 and 50 K. Figure 6 shows representative spectra of solid **1** (A) and of **1** dissolved in toluene (B). The toluene sample exhibits a signal at $g = 8.6$ that belongs to a Kramers doublet with highly anisotropic g values.[23] Powder **1** exhibits a broader feature centered at $g = 8.9$; the signal around $g = 4.3$ most likely belongs to a minor $S = {}^5/_2$ contaminant, because it accounts for less than 1% of the total spin concentration (see Supporting Information). This assignment is consistent with the low-temperature Mössbauer spectra, which reveal no species other than **1**. Moreover, its absence in the solution sample shows that the two signals observed in the powder sample belong to two different spin systems. The $g = 8.9$ feature in the solid sample is substantially broadened as a result of unresolved spin−spin interactions (the shortest Fe−Fe distance in the crystal structure is 8.6 Å). For a doublet with $g_x \gg g_y, g_z$, the area under the EPR signal at g_x is proportional to $g_y^2 + g_z^2$.[24] The observation of a signal at g_x, thus, implies that g_y and $g_z \neq 0$. The $g = 8.6$ and 8.9 signals were not observed in parallel mode EPR, supporting the above conclusion that both features belong to a Kramers system.

Discussion

***g* Values and B_{int}.** To gain insight into the electronic structure of LFe^{I}HCCPh, we have performed DFT and crystal field calculations. The structural models used in the DFT calculations are depicted in Figure S.2 (Supporting Information) and yield an electronic ground state of which the $3d^7$ component is approximately of the form $|(xy)^2(z^2)^2(yz)^{\alpha}(x^2-y^2)^{\alpha}(xz)^{\alpha}|$ (Figure 7C). As expected for a ground state, TD-DFT calculations for this state yield exclusively positive excitation energies; the lowest energies correspond to d−d transitions and are listed in the first

(22) Schulz, C. E.; Nyman, P.; Debrunner, P. G. *J. Chem. Phys.* **1987**, *87*, 5077−91.

(23) On one occasion, the toluene sample (flame-sealed EPR tube) melted for a few seconds during transfer. Upon refreezing, microcrystals formed, which produced a multitude of single-crystal-type resonances down to at least $g = 1$; these resonances shifted when the sample tube was rotated in the EPR cavity. Thus, the feature at $g = 8.6$ belongs to a doublet that has g values extending to at least $g = 1$.

(24) Aasa, R.; Vanngard, T. *J. Magn. Res.* **1975**, *19*, 308−315.

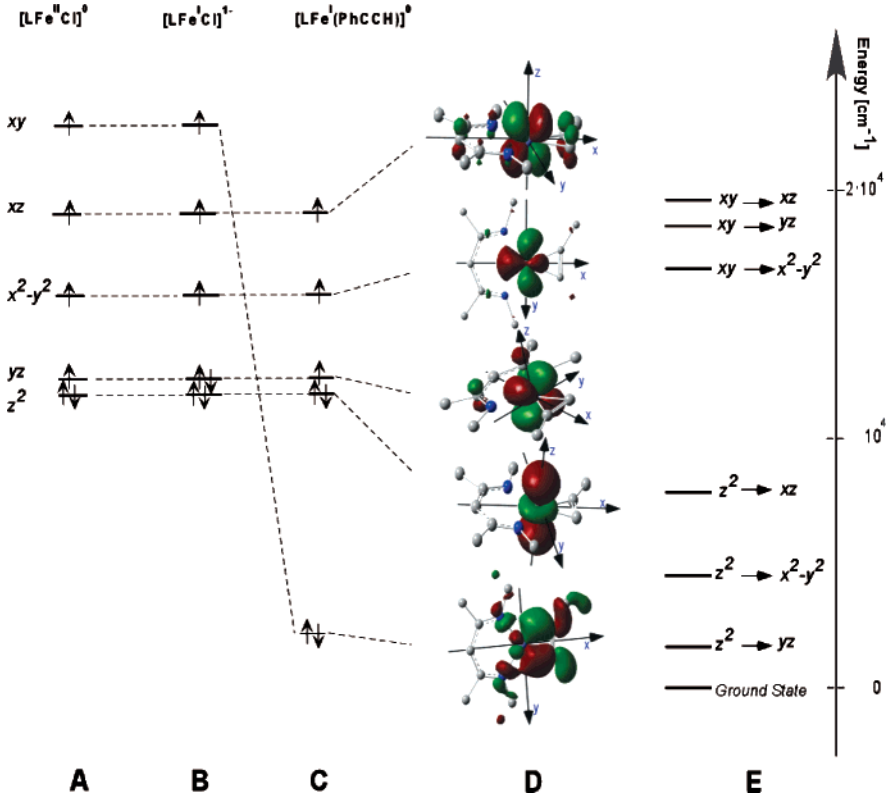

Figure 7. **A**−**C**: Schematic representations, for the purpose of conveying the arguments presented in the text, of the electronic ground-state configurations and orbital level schemes for $[LFe^{II}Cl]^0$, the hypothetical complex $[LFe^{I}Cl]^{1-}$, and $[LFe^{I}(HCCR)]^0$. The Cartesian coordinates used in the definition of the orbitals are indicated in panel D. In panels A−C, z^2 and *yz* are represented by quasi-degenerate levels to account for the unquenched orbital momentum observed in $[LFe^{II}Cl]^0$ and $[LFe^{I}(HCCR)]^0$. The ligand field and d−d repulsion contributions to the excitation energies in $[LFe^{I}(HCCR)]^0$ for $\{(z^2)^\beta \rightarrow (d')^\beta\}$ ($d' = yz$, x^2-y^2, and *xz*) are specified in the Supporting Information. *xy* is singly occupied in panels A and B but doubly occupied in C because of the lowering of the *xy* level by donation of *xy* electron density into the acetylene π^* orbital (see text). **D**: Isosurface plots of the 3d-type orbitals for the β electrons in C; associations are indicated by dashed lines. The plots of the *occupied* $(z^2)^\beta$ (β HOMO) and $(xy)^\beta$ are the DFT molecular orbitals with predominant z^2 and *xy* character, respectively. The plots for the *virtual* orbitals, $(d')^\beta = (yz)^\beta$, $(x^2-y^2)^\beta$, and $(xz)^\beta$, were obtained from the TD-DFT solutions in which $\{(z^2)^\beta \rightarrow (d')^\beta\}$ appears as the leading excitation by a procedure described in the Supporting Information. **E**: Lowest six $(d)^\beta \rightarrow (d')^\beta$ excitation energies obtained by TD-DFT for $[LFe^{I}(HCCMe)]^0$. The energy gap separating the sets $\{(z^2)^\beta \rightarrow (d')^\beta\}$ and $\{(xy)^\beta \rightarrow (d')^\beta\}$ reflects the separation between the z^2 and *xy* orbital levels indicated in panel C. For clarity, the superscript β has been omitted in E.

column of Table S.3 (Supporting Information). Figure 7 shows schematic orbital level schemes. Figure 7A corresponds to $[LFe^{II}Cl]^0$, the complex studied by Andres et al.[9a] The magnetic properties of this complex are determined by the (near) degeneracy of two configurations obtained by placing the highest β electron in either z^2 or *yz*. These configurations mix by spin−orbit coupling to produce a nearly degenerate ground doublet (corresponding to the magnetic quantum number $M_S = \pm 2$) with essentially unquenched orbital angular momentum ($\langle L_z \rangle \approx \pm\sqrt{3}$).[9] Figure 7B shows the levels of the fictitious compound $[LFe^{I}Cl]^-$. It can be seen that the most effective mixing by spin−orbit coupling involves the two configurations related by excitation of a β electron from *yz* to x^2-y^2. These two configurations are expected to be well-separated in energy and, thus, would not appreciably mix by spin−orbit coupling. Consequently, one might expect an $S = {}^3/_2$ ground state with essentially quenched angular momentum and moderate zero-field splitting, such as $|D| < 15$ cm^{-1}.[25]

When we first noticed, for $[LFe^{I}HCCPh]^0$, the unquenched orbital angular momentum, in evidence by the large and positive B_{int} together with the presence of an isolated spin doublet, we suspected that a different pair of degenerate orbital configurations than that in $[LFe^{I}Cl]^-$ was involved. Interestingly, TD-DFT reveals that the unquenching of the orbital angular momentum by spin−orbit coupling involves the same $z^2 \rightarrow yz$ excitation in both $LFe^{I}HCCR$ and $LFe^{II}X$ ($X = Cl^-$, CH_3^-) because of a dramatic lowering of the energy of the *xy* orbital (this is illustrated in Figure 7). The $\{z^2 \rightarrow yz\}$ excitation energy remains small, presumably because z^2 is essentially nonbonding and *yz* interacts primarily with the diketiminate nitrogen atoms. Our experimental results for $[LFe^{I}HCCPh]$ and $[LFe^{II}X]$[9] indicate that the energy gap between the two critical electronic configurations (without consideration of spin−orbit coupling) must be at least 1 order of magnitude smaller than indicated by TD-DFT. This should not come as a surprise considering that excited-state energies obtained by TD-DFT may have errors of 1500 cm^{-1};[26] moreover, our models are simplified by assuming higher symmetries imposed by computational requirements. In the following, we will argue that the mixing

(25) A high-spin $S = {}^3/_2$ system without orbital degeneracies would exhibit an effective moment $\mu_{eff} = 3.9\ \mu_B$ for $g_x = g_y = g_z = 2$. The powder-averaged moment of the ground doublet of solid **1** would be $\approx 4.5\ \mu_B$. A slightly smaller g_x for the latter case or larger g_i for the former case, would virtually yield indistinguishable results in magnetization studies. Such studies require levels of sample purity presently not attainable for **1**.

(26) Wiberg, K. B.; Stratmann, R. E.; Frisch, M. J. *Chem. Phys. Lett.* **1998**, *297*, 60.

of two nearly degenerate configurations by spin−orbit coupling is responsible for the electronic properties elicited by Mössbauer and EPR spectroscopy. We refer to these configurations as $\{z^2\}$ and $\{z^2 \rightarrow yz\}$, the latter being obtained from $\{z^2\}$ by excitation of a β electron from z^2 to yz.

Suppose that $\{z^2\}$ and $\{z^2 \rightarrow yz\}$ are degenerate. In this case, the levels are maximally mixed by spin−orbit coupling and the β HOMO can be replaced by complex orbitals of the form $\varphi_{\pm} = (z^2 \pm iyz)/\sqrt{2}$, where $i = \sqrt{-1}$. The spin−orbit coupling operator is diagonal in the basis $\{\varphi_{\pm}{}^{\alpha}, \varphi_{\pm}{}^{\beta}\}$, provided the electronic spin is quantized along x. The interaction yields doublets for which $S = {}^3/_2$ and M_S are good quantum numbers. Because the one-electron spin−orbit coupling constant is positive, $\zeta_{\text{free ion}} = 357$ cm^{-1},[27] the resulting $|S = {}^3/_2, M_S = \pm{}^3/_2\rangle$ doublet is lowest in energy, and it is this doublet that yields the EPR and Mössbauer data reported in the Results; in the above expression for the β HOMO, the $\pm$ signs correlate with $M_S = \mp{}^3/_2$. The ground doublet is separated by an energy gap of $\zeta/\sqrt{3}$ from the excited doublet $|S = {}^3/_2, M_S = \pm{}^1/_2\rangle$. Accordingly, the energy gap between the two lowest Kramers doublets (the "zero-field splitting" of the $S = {}^3/_2$ quartet) is approximately 170 cm^{-1} (using a covalently reduced $\zeta = 300$ cm^{-1}), which overlaps with the Δ range deduced from the analysis of the relaxation properties of the Mössbauer spectra. The predicted limits are lower when $\{z^2\}$ and $\{z^2 \rightarrow yz\}$ have different energies.

To compute the effective g values of the doublet, we have calculated the matrix elements of the Zeeman operator $\mathscr{H}_Z = \beta(\mathbf{L} + 2\mathbf{S})\mathbf{B}$ in the subspace of the $|S = {}^3/_2, M_S = \pm{}^3/_2\rangle$ doublet and then equated these matrix elements, as is commonly done, to those obtained with the Zeeman operator $\mathscr{H}_Z = \beta\mathbf{S}'\cdot\mathbf{g}\cdot\mathbf{B}$ acting in the subspace of the fictitious spin $S' = {}^1/_2$. The effective g values (g_x, g_y, g_z), in the degenerate case, are (9.5, 0, 0) for the lowest doublet $[g_x = 2(3 + \sqrt{3})]$ and (5.5, 0, 0) for the excited doublet at energy $\zeta/\sqrt{3}$. Smaller values for g_x are obtained in the nondegenerate case;[9] moreover, g_y and g_z for the *excited* doublet then differ from zero. The value $g_x = 9.5$ is close to the $g_x = 8.9$ value observed by EPR for solid **1**. Deviations from true degeneracy of $\{z^2\}$ and $\{z^2 \rightarrow yz\}$ might be the reason for the observation of a smaller g_x, although we should not unreasonably stretch the simplified model and attempt to determine this deviation. Clearly, as described in ref 9, higher lying configurations, such as $\{z^2 \rightarrow xz\}$, will also interact with $\{z^2\}$ by spin−orbit coupling. In fact, the observation that the ground doublet has g_y, $g_z \neq 0$, but g_y, $g_z < 0.3$, indicates the influence of such states. The 8.0 T spectrum recorded at 150 K (Figure S.1, Supporting Information) had to be simulated with uniaxial magnetic hyperfine interactions and a reduced value of g_x. The above considerations show that the first excited doublet is also uniaxial, with B_{int} along x. Hence, the 150 K Mössbauer spectrum will exhibit uniaxial magnetic properties even when the excited doublet is significantly populated. Moreover, because g_x for the excited state is smaller (= 5.5), the effective g_x value of the system will be smaller at 150 K, as indicated by the analysis of the 8.0 T spectrum.

The internal magnetic field, B_{int}, that is, the magnetic field generated by the electrons at the ^{57}Fe nucleus, comprises a Fermi contact (B_{FC}), orbital (B_{L}), and spin dipolar (B_{SD}) contribution. Because the ground doublet is uniaxial along x, our experiments provide the internal field along this direction, $B_{\text{int},x}$. The Fermi contact contribution is given by $B_{\text{FC},x} = \kappa P\langle S_x\rangle \approx -32$ T, where κ is a numerical factor of about 0.35 and $P = 2\beta_B\langle r^{-3}\rangle_{3d} \approx 60$ T.[28] B_{FC} has a negative sign (i.e., it is opposed to the applied magnetic field) as $\langle S_x\rangle$ is negative in the lowest Zeeman level ($M_S = -{}^3/_2$). The orbital contribution along x is given by $B_{\text{L},x} \approx P\langle L_x\rangle$ and has a positive sign. B_{L} is negligibly small compared to B_{FC} in the large majority of the high-spin iron complexes because the orbital angular momentum is virtually quenched by the crystal field. However, [LFe$^{\text{I}}$HCCR], like LFe$^{\text{II}}$X reported earlier,[9] is an exception. The expectation values of L_x in the $M_S = \pm{}^3/_2$ components (quantized along x) of the ground state, in which there is a β electron in the complex orbital $(z^2 \mp iyz)/\sqrt{2}$, are equal to $\pm\sqrt{3}$, yielding $B_{\text{L},x} = \mp P\sqrt{3}$. Hence, $B_{\text{L},x} \approx 100$ T is positive in the lowest Zeeman level, $-{}^3/_2$. The spin dipolar term, evaluated for the d^7 ground configuration obtained in the presence of spin−orbit coupling between z^2 and yz, yields only a small contribution: $B_{\text{SD},x} = P/14 \approx +4$ T. The resulting internal field, $B_{\text{int},x} = B_{\text{FC},x} + B_{\text{L},x} + B_{\text{SD},x} \approx +72$ T, is in good agreement with the experimental value $B_{\text{int}} = +68.8(3)$ T.

Nature of the Iron−Acetylene Interaction. The isosurface plot of the "*xy*" orbital (see Figure 7) shows that the remarkable lowering of the *xy* level, from the top of the level scheme for [LFe$^{\text{II}}$Cl]^0 to the bottom of the scheme for [LFe$^{\text{I}}$HCCR]^0, is due to the donation of *xy* electron density into one of the π^* orbitals of the acetylene moiety of the HCCR ligand. From this observation, we conclude that $|(xy)^2(z^2)^2(yz)^{\alpha}(x^2-y^2)^{\alpha}(xz)^{\alpha}|$ is the most appropriate 3d^7 configuration for describing the electronic state of Figure 7C. The ground configuration belongs to the ^{4}F ground manifold of the free Fe$^{\text{I}}$ ion and minimizes the electronic repulsion energy between the 3d electrons. The level scheme in Figure 7E presents the excitation energies for the β electrons as obtained by TD-DFT. The expressions for the excitation energies are listed in Table S.3 (Supporting Information) in terms of 3d crystal-field energies (ϵ_i), which describe the influence of the ligands on the 3d orbital energies, and Racah parameter B, which describes the Coulomb repulsions between the 3d electrons. The differences of the excitation energies for $\{xy \rightarrow x^2-y^2\}$ and $\{xy \rightarrow yz\}$ $[\epsilon(x^2-y^2) - \epsilon(yz) - 9B]$ and for $\{z^2 \rightarrow x^2-y^2\}$ and $\{z^2 \rightarrow yz\}$ $[\epsilon(x^2 - y^2) - \epsilon(yz) + 9B]$ differ by 18B. This latter difference is estimated to be 4500 cm^{-1} from TD-DFT excitation energies (Table S.3, Supporting Information) and implies that $B \approx 250$ cm^{-1}. This value is rather small compared to the free ion value of this parameter ($B \approx 1000$ cm^{-1}).[29] The B value is essential to ensure that the contribution to the $\{z^2 \rightarrow yz\}$ excitation energy arising from the

(27) Bendix, J.; Brorson, M.; Schäffer, C. E. *Inorg. Chem.* **1993**, *32*, 2838−2849.

(28) Lang G. *Q. Rev. Biophys.* **1970**, *3*, 1−59.

electronic repulsions of the 3d electrons (3*B*) is small in LFeHCCPh. Because Cl^- and HCCPh interact only weakly with the *yz* orbital, it is not surprising that the *yz* and z^2 orbitals remain at very similar energies under exchange of these ligands. Because $\epsilon(yz) - \epsilon(z^2)$ in $LFe^{II}Cl$ is small, the corresponding excitation energy in LFeHCCPh [$\epsilon(yz) - \epsilon(z^2) + 3B$] is expected to be small as well. Using the orbital energies and *B* values listed in Table S.3 of the Supporting Information as a guideline, the $\{z^2 \rightarrow yz\}$ excitation energies for the two complexes are estimated to differ by a few hundred wavenumbers.[30] Given these variations, finding a quasi-degeneracy within ~100 cm^{-1}, such as that required to obtain the orbital magnetic moment observed in LFe^{I}-HCCPh, is somewhat fortuitous.[31]

The formal iron oxidation state in LFe(HCCPh), based on net charge (0) and the formal charges of diketiminate (−1) and phenylacetylene (0), is Fe^{I}. The *xy* orbital of Fe^{I} is formally doubly occupied but has a DFT Mulliken population of only 1.2 electrons [i.e., 0.6 electrons in the spin−orbitals $(xy)^{\alpha}$ and $(xy)^{\beta}$ each] due to substantial back-donation of *xy* into a π^* orbital of phenyl acetylene: $c_1(xy) + c_2(\pi^*)$, where $c_1^2 + c_2^2 \approx 1$ for $\langle xy|\pi^*\rangle \approx 0$. Because Mulliken charges are usually smaller than formal charges, the value for the charge of Fe^{I} (+1.1) suggests the involvement of oxidation states higher than Fe^{I}. The *xy* population corresponds to the mixing coefficients $c_1 \approx \sqrt{0.6}$ and $c_2 \approx \sqrt{0.4}$. The DFT ground state can be expanded as a superposition of formal oxidation states (see Supporting Information).

$$c_1^2|L^{1-}Fe^{I}(HCCPh)^0\rangle + c_2^2|L^{1-}Fe^{III}(HCCPh)^{2-}\rangle + \sqrt{2}c_1c_2|\langle L^{1-}Fe^{II}(HCCPh)^{1-}\rangle \quad (3)$$

The first term represents a high-spin Fe^{I} configuration, the second term is associated with intermediate-spin Fe^{III}, and the third term gives an Fe^{II} configuration with a Heitler−London bond between an unpaired electron in *xy* and a radical electron in π^*. The corresponding probabilities are $c_1^4 \approx 0.36$ (Fe^{I}), $c_2^4 \approx 0.16$ (Fe^{III}), and $2c_1^2c_2^2 \approx 0.48$ (Fe^{II}). The average charge of HCCPh in eq 3 is −0.8 and is equal to the Mulliken charge for this moiety obtained by DFT. Assuming a diketiminate charge of −1, the Fe charge estimated from eq 3 is +1.8; however, the actual Mulliken charges are −0.3 (diketiminate) and +1.1 (Fe). These values indicate that the electron loss of Fe to HCCPh is almost compensated by donation of 0.7 electrons from L to Fe: $L^{1-} \overset{0.7-}{\rightarrow} Fe^{1+} \overset{0.8-}{\rightarrow} (HCCPh)^0$, which yields $L^{0.3-}Fe^{1.1+}(HCCPh)^{0.8-}$ in which 0.7 electrons have been effectively shifted from L to HCCPh.

The C−C bond order in LFe(HCCPh) is calculated to be 2.6 and corresponds to the aforementioned donation of slightly less than one electron to the alkyne ligand. Consistent with the intermediate value calculated for the bond order in LFe(HCCPh), the C−C stretching frequency (calcd: 1758 cm^{-1}; exptl: 1720 cm^{-1}) and the C−C distance (calcd: 1.29 Å; exptl: 1.27 Å) are each intermediate between the values expected for double and triple bonds (cf. Supporting Information). In the literature, two classes of metal−acetylene complexes have been discussed: one class in which σ donation dominates the bonding and another class in which π back-donation causes charge transfer from the metal to the acetylene ligand.[32] LFe(HCCPh) has properties more consistent with the second class: (a) the ligand triple bond is weakened and lengthened, (b) the C≡C−X (X=H, R) angle is bent, and (c) the C≡C stretching frequency is lowered by roughly 400 cm^{-1} from the free acetylene. The vibrational frequencies for the C≡C bond, the C≡C distance, and the C≡C−C angle in LFe(HCCPh) are consistent with numerous literature complexes in class b (see Supporting Information for details).

In conclusion, this paper reports the first comprehensive Mössbauer and EPR studies of a formally high-spin Fe^{I} complex. Complex **1** and $LFe^{II}Cl$ both produce ground-state configurations with (near) orbital degeneracies, yielding isolated ground doublets (a quasi-doublet, in the case of $LFe^{II}Cl$)[9] with uniaxial magnetic properties. These initially puzzling observations were rationalized by DFT calculations that show that back-bonding into an empty π^* orbital of the acetylene moiety of **1** lowers the energy of *xy* such that the orbitals that determine the magnetic properties of the two complexes by spin−orbit mixing are essentially the same. The σ dative bonding between the metal and the acetylene ligand, involving x^2-y^2 and one of the C≡C π orbitals, renders the complex essentially three-coordinate. The DFT calculations indicate a substantial charge transfer to the acetylene moiety and yield a C−C bond length and stretching frequency that are consistent with the experiment.

Acknowledgment. This work was supported by NSF Grants MCB-0424494 (E.M.) and CHE-0134658 (P.L.H.).

Supporting Information Available: High-temperature Mössbauer spectra of **1**, EPR information, details of DFT calculations, and crystal field analysis. Crystallographic data is in CIF format. This material is available free of charge via the Internet at http://pubs.acs.org.

IC050321H

(29) The partial Fe^{II} character conferred on the formal Fe^{I} site in $[LFe(HCCPh)]^0$ by π^* back-donation gives rise to a reduction of the *B* value obtained from the $3d^7$-based analysis presented above. The population of the *xy* orbital (1.2) is close to the *xy* population in high-spin Fe^{II} (1.0) and reduces the dependence of the $\{z^2 \rightarrow yz\}$ and so forth transition energies on the Coulomb repulsions between the 3d electrons. The Fe^{II} configuration in eq 3 also involves an intermediate-spin Fe^{II} contribution, introducing energy terms depending on Racah parameter *C*. This issue has not been further analyzed here.

(30) The TD-DFT results for the $\{z^2 \rightarrow yz\}$ excitation energy are too large in both complexes but are within the error margin reported for TD-DFT excitation energies.

(31) The degeneracies referred to here are obtained without spin−orbit coupling.

(32) (a) Hartley, F. R. *Angew. Chem., Int. Ed. Engl.* **1972**, *11*, 596−606. (b) Boston, J. L.; Grim, S. O.; Wilkinson, G. *J. Chem. Soc.* **1963**, 3468−3470. (c) The wealth of computational work on metal−acetylene complexes has been reviewed recently: Frenking, G.; Fröhlich, N. *Chem. Rev.* **2000**, *100*, 717−774.